frontiers | Frontiers in Water

TYPE Original Research
PUBLISHED 07 August 2025
DOI 10.3389/frwa.2025.1635275

Check for updates

OPEN ACCESS

EDITED BY
Venkatramanan Senapathi,
National College, Tiruchirappalli, India

REVIEWED BY
Sivakumar Karthikeyan,
Alagappa University, India
Baoyuan Zhang,
Nanjing Agricultural University, China

*CORRESPONDENCE
Yancang Wang
✉ yancangwang@163.com

RECEIVED 26 May 2025
ACCEPTED 16 July 2025
PUBLISHED 07 August 2025

CITATION
Lv W, Wang Y, Cao H, Cheng P, Gu X, Ma Z, Li M, Tang R, Zhao Q, Li X, Zhang L and Liu S (2025) Proximal remote sensing of dissolved organic matter in aqua-culture ponds via multi-temporal spectral correction. *Front. Water* 7:1635275.
doi: 10.3389/frwa.2025.1635275

Proximal remote sensing of dissolved organic matter in aqua-culture ponds via multi-temporal spectral correction

Wenxu Lv[1], Yancang Wang[1]*, Huiqiong Cao[1], Peng Cheng[1], Xiaohe Gu[2], Zhuoran Ma[3], Mengjie Li[1], Ruiyin Tang[1], Qichao Zhao[1], Xuqing Li[1], Lan Zhang[1] and Shuaifei Liu[1]

[1]College of Remote Sensing Information Engineering, North China Institute of Aerospace Engineering, Langfang, China, [2]Research Center of Information Technology, Beijing Academy of Agriculture and Forestry Sciences, Beijing, China, [3]Department of Human Centred Computing, Faculty of Information Technology, Monash University, Melbourne, VIC, Australia

Dissolved organic matter (DOM) is a critical indicator of aquatic environmental quality, and its concentration affects the quality of aquaculture products. Integrating unmanned aerial vehicle (UAV)-based multispectral data with machine learning algorithms enables accurate estimation of DOM. However, the stability of models in different periods—such as those affected by seasonal variations and environmental condition changes—is the key factor affecting their application. This study employed a spectral correction method to unify multi-temporal datasets. Estimation models were constructed using the 2023 dataset with Light Gradient Boosting Machine, Extreme Gradient Boosting, and Random Forest algorithms, and their cross-year performance was validated on the 2024 dataset through transfer learning. Results showed that models trained on corrected data outperformed those using raw spectra, with an average R^2 increase of 15.67%, and reductions of 10.27% in RMSE and 6.44% in MAE on the test set. After transfer learning optimization, the model using the corrected spectrum still exhibited superior performance in 2024. Compared with the original spectrum, an average R^2 improvement of 30.67%, along with reductions of 17% in RMSE and 11.67% in MAE. Among the three algorithms, the Random Forest model yielded the best performance, with an R^2 of 0.82, RMSE of 3.1 mg/L, and MAE of 2.37 mg/L on the test set. The proposed approach in this study effectively mitigates the temporal impact on model performance and enhances the temporal generalization capability of DOM estimation models.

KEYWORDS

UAV-based multispectral imagery, dissolved organic matter, multi-temporal, spectral correction, transfer learning, machine learning

1 Introduction

Freshwater aquaculture represents a vital component of the global food production system. With the increasing global population and rising demand for high-quality protein, its scale and market demand have steadily increased (Naylor et al., 2021). Beyond serving as a crucial source of dietary protein, freshwater aquaculture contributes significantly to economic, environmental, and social benefits (Prasad et al., 2019; Xu et al., 2024). In China, the aquaculture sector has emerged as a strategic driver of economic growth and structural optimization within the agricultural industry (Duan et al., 2025). However, such rapid development has also brought forth challenges related to environmentally sustainable development, particularly in water quality monitoring and management (Liu et al., 2023; Zhang et al., 2015). Enhancing the accuracy and efficiency of water quality monitoring has become essential for ensuring the ecological integrity of aquaculture ponds and fostering sustainable development in the sector. The integration of spectral technologies with Unmanned Aerial Vehicles (UAVs) offers new opportunities for precision aquaculture. These technologies not only improve production efficiency and reduce costs but also contribute to environmental conservation and enhance decision-making capacity. As such, they provide a scientific foundation for sustainable pond management and demonstrate substantial practical value in freshwater aquaculture.

Conventional manual sampling and laboratory analysis methods provide accurate data but suffer from high costs and inefficiency in real-time large-scale monitoring, rendering them inadequate for modern aquaculture's dynamic monitoring demands. With the widespread application of satellite remote sensing, hyperspectral, and multispectral technologies, substantial technical support and research directions have been provided for water quality monitoring (Bean et al., 2017; Sagan et al., 2020). Satellite-based water quality monitoring has emerged as an efficient solution, enabling long-term tracking and large-scale observation across aquatic environments (Han et al., 2023; Peng et al., 2022).

Nevertheless, satellite remote sensing is restricted by its spatial resolution and its capacity to characterize shallow water regions (Liu et al., 2019), which restricts further improvements in monitoring accuracy. Hyperspectral remote sensing, with its rich spectral information, enables molecular-level identification and precise quantitative analysis of specific chemical substances in water bodies. This technology provides distinct advantages for monitoring DOM and other complex water quality parameters (Luo et al., 2023). Nevertheless, the high cost and complex data processing requirements of hyperspectral remote sensing limit its practical application.

Multispectral remote sensing technology achieves a favorable balance among spectral band selection, spatial resolution, and cost, and has gradually established an important tool for estimating water quality parameters. Multispectral sensors can resolve key spectral information from water bodies, enabling high-resolution monitoring of water quality parameters through the construction of spectral features combined with machine learning algorithms, while effectively capturing the spatial heterogeneity of aquatic environments. Compared with traditional satellite remote sensing, UAV-based remote sensing provides superior spatial and temporal resolution, allowing for the acquisition of high-accuracy, high-frequency data under low-altitude flight conditions, significantly enhancing both the precision and timeliness of monitoring efforts (Zheng et al., 2024). Relative to hyperspectral remote sensing, multispectral imaging is more cost-effective, operationally efficient, and easier to process, making it particularly suitable for fine-scale, high-resolution monitoring scenarios such as freshwater aquaculture ponds. Furthermore, UAVs equipped with multispectral sensors have extended the applicability of multispectral remote sensing by enabling the spatiotemporal tracking of water quality parameters with greater flexibility. When combined with machine learning algorithms, this integration allows for the accurate characterization of dynamic water quality patterns, effectively addressing the limitations of conventional monitoring methods under high-frequency, high-accuracy demands.

Dissolved organic matter (DOM) is a key optically active constituent in aquatic environments, and its concentration and spectral characteristics are widely used to assess water quality and ecological balance (Zhang et al., 2014; He et al., 2022). As a critical indicator of water quality, DOM influences algal growth and the complexation behavior of metal ions and plays a direct role in the transport and transformation of aquatic pollutants. Excessive DOM concentration is recognized as one of the major contributors to eutrophication (Chen and Li, 2021; Li et al., 2021). Although electrochemical methods provide accurate measurements of DOM concentration, the need for time-consuming sample pretreatment and complex analytical procedures often compromises the efficiency and reliability of the results, rendering them unsuitable for real-time and large-scale monitoring (Bi et al., 2013). In contrast, the integration of spectral indices, spectral shape analysis, and intelligent algorithms offers a promising solution for capturing the spatiotemporal dynamics of DOM. This approach enables high-frequency, high-accuracy monitoring and enhances the feasibility of near-real-time DOM assessments in aquatic environments.

With the continuous advancement of remote sensing technology, its application in monitoring DOM in aquatic environments has received increasing attention. In satellite remote sensing studies, Griffin et al. (2011) estimated CDOM concentrations in rivers and their tributaries using empirical algorithms, revealing that previous estimates of DOM flux may have underestimated actual outputs. Kutser et al. (2005) evaluated the applicability of various satellite sensors for monitoring CDOM concentrations in Nordic lakes and found that the 565–660 nm bands of the ALI sensor were highly correlated with CDOM absorption coefficients ($R^2 = 0.84$). In UAV-based hyperspectral research, Galešić Divić et al. (2026) developed regression models for CDOM concentration based on UAV hyperspectral data, achieving a coefficient of determination (R^2) greater than 0.90. Seidel et al. (2020) optimized UAV imaging spectroscopy extraction methods and constructed a predictive model using the 470–850 nm spectral range, yielding an R^2 of 0.75 for CDOM estimation. UAV-based multispectral technology, with its flexibility and ultra-high spatial resolution, presents distinct advantages for monitoring DOM concentrations. For instance, Yao et al. (2024) developed and optimized support vector regression (SVR) models for predicting concentrations of various typical water quality parameters, achieving R^2 values exceeding 0.80. Chen G. et al. (2024) estimated DOM concentrations using UAV multispectral data, with the random forest model performing best and reaching an R^2 of 0.81. However, the temporal generalization ability of water quality parameter estimation models remains limited due to varying illumination conditions, atmospheric factors, and surface cover changes across different acquisition periods. To address these challenges, this study proposes the spectral correction approach that adjusts spectral deviations caused by changes in solar irradiance and solar zenith angle across time, thereby enhancing the consistency and applicability of multispectral imagery. Meanwhile, this study introduces the transfer learning approach to improve the temporal adaptability and generalization capability of UAV-based DOM monitoring models, thereby providing more scientific and reliable technical support for dynamic water quality monitoring in freshwater aquaculture ponds.

This study proposes a multispectral estimation method for DOM in ponds, coupling spectral correction with the transfer learning approach. The specific objectives are: (1) to verify the performance of the spectral correction method in adjusting UAV multispectral imagery from different time periods; (2) to assess the effectiveness of the spectral correction method in enhancing the temporal generalization ability of DOM concentration estimation models; (3) to investigate the combined performance of spectral correction and the transfer learning approach in improving the temporal generalization ability of water quality parameter estimation models, and to construct a stable, reliable, accurate, and temporally generalizable estimation model.

2 Materials and methods

2.1 Overview of the study area

This study was conducted at a Chinese mitten crab (*Eriocheir sinensis*) aquaculture base in Gaochun District, Nanjing City, Jiangsu Province, China (Figure 1). Gaochun District, situated in the southwestern part of Jiangsu and the southern part of Nanjing, is one of the well-known freshwater aquaculture regions in China and is characterized by a typical northern subtropical humid climate. The area features abundant water resources, distinct seasons, ample precipitation, and a wide annual temperature range with sufficient sunlight. Gaochun has an average annual temperature of 17.5°C and an average annual precipitation of approximately 1,010 mm. The terrain is predominantly flat with interspersed hills and uplands—rolling low hills dominate the eastern region, while the western part consists of lake basins and plains with a dense water network—providing highly favorable natural conditions for freshwater aquaculture. The total aquaculture area in Gaochun District exceeds 200,000 mu (approximately 13,300 hectares), with an annual crab production close to 20,000 tons, making it an ideal site for research on water quality parameter monitoring in freshwater aquaculture ponds. This study selected a Chinese mitten crab breeding site located on the western side of Gucheng Lake as the experimental base, which includes 36 aquaculture ponds covering an area of approximately 1,600 mu (about 107 hectares), with a total cultured crab population of 112,200 individuals.

2.2 Data acquisition and processing

The primary cultivation period for Chinese mitten crabs extends from March to October. Within this period, April to June marks the active growth phase, July to August corresponds to the rapid growth stage, and September to October represents the maturation phase. During this period, the deterioration of the aquatic environment can lead to slow growth or even mortality in crabs. Therefore, this period is considered crucial for pond water quality management. This study

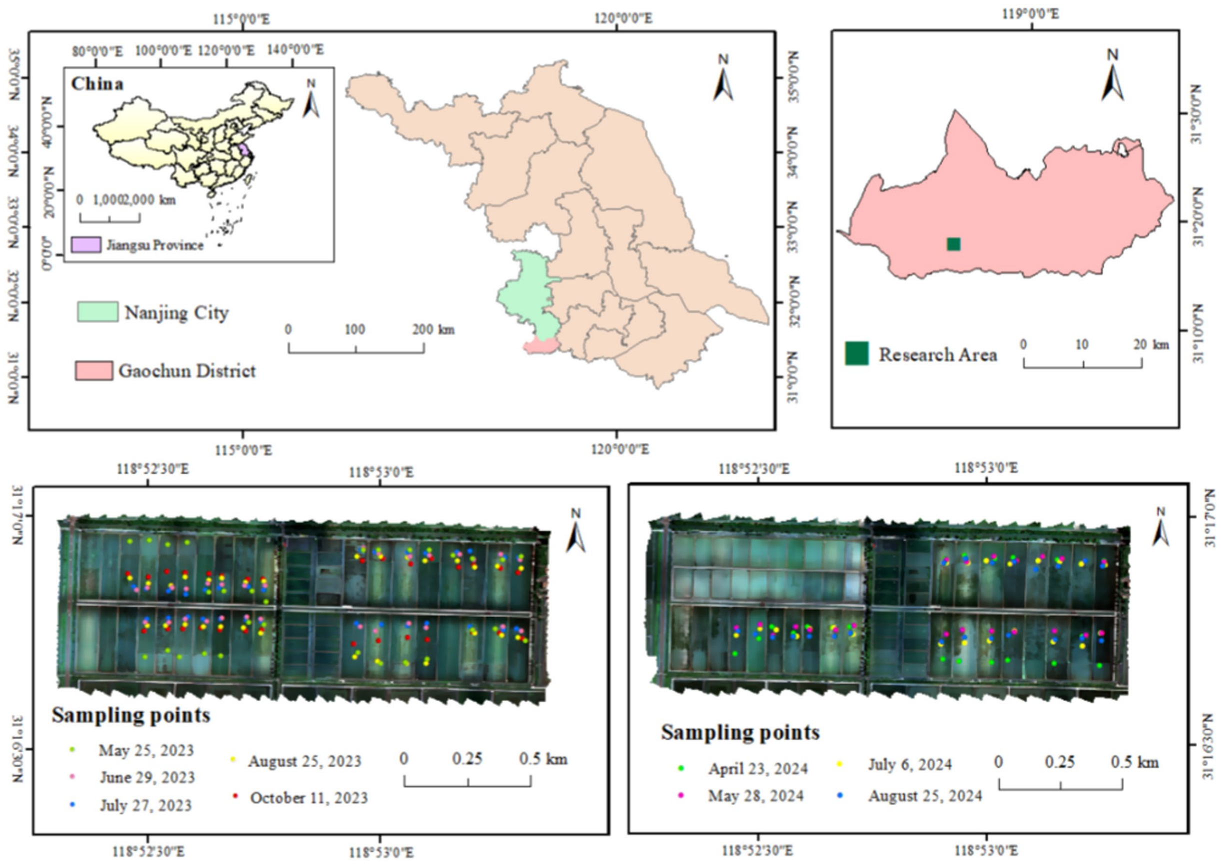

FIGURE 1
Geographic location of the study area and distribution of sampling sites.

carried out field experiments from May to October 2023 and from April to August 2024, during which 238 water quality samples were gathered, including 150 data sets from 2023 and 88 from 2024. The spatial layout of the sampling locations is presented in Figure 1.

2.2.1 DOM data

To make sure the representativeness of the sampling points and avoid the influence of nearshore pollution or localized environmental factors, the sampling was conducted in aquaculture ponds located farther from the shore. The sampling depth was standardized at approximately 30 cm below the water surface. The "five-point composite sampling method" was employed to guarantee the uniformity and representativeness of the collected water samples.

Prior to sampling, each sampling bottle and cap were rinsed three times with the water to be sampled to prevent contamination. Immediately after collection, water samples were transferred into 500 mL opaque containers and thoroughly mixed to prevent the influence of light on DOM and avoid photodegradation or other reactions. To maintain sample freshness and accuracy, the samples were first stored in insulated boxes with ice packs under low-temperature and light-avoiding conditions. They were then promptly transported to the testing laboratory for chemical analysis within 8 h. In the laboratory, a suitable oxidizing agent was put into the water samples to oxidize the organic carbon into carbon dioxide, which was subsequently measured via the non-dispersive infrared (NDIR) spectroscopy method. The NDIR technique indirectly determines the DOM concentration by detecting the absorption characteristics of carbon dioxide. The entire analysis strictly followed the national standard GB/T 5750.7-2006 Standards for Drinking Water Quality – Part 7: Methods for Organic Substance Analysis, ensuring the accuracy and reliability of the experimental results.

2.2.2 UAV multispectral data

In this study, nine field experiments were conducted, during which multispectral drone imagery was collected simultaneously. The ground sampling dates were May 25, 2023; June 29, 2023; July 27, 2023; August 25, 2023; October 11, 2023; April 23, 2024; May 28, 2024; July 6, 2024; and August 25, 2024. The time span between the first and the last experiment was approximately 1 year and 2 months. A DJI Phantom 4 UAV Multispectral was used as the data acquisition platform for periodic multispectral imaging over freshwater aquaculture ponds (Figures 2a,b). The UAV has an integrated multispectral imaging system that includes one RGB camera and five narrowband multispectral sensors (Table 1), allowing for the precise collection of high-resolution spectral data. Its robust flight performance—With a maximum flight duration of 27 min, its control range extends up to 7 km—ensures efficient data acquisition. The integrated sunlight sensor on top of the UAV captures solar irradiance to compensate for lighting variations, thereby improving the accuracy of reflectance measurements. In addition, the UAV includes a TimeSync system, centimeter-level Real-Time Kinematic (RTK) positioning, and the D-RTK 2 high-precision GNSS mobile station. Combined with network RTK technology, this setup provides highly accurate geolocation information and ensures the spatial consistency of imagery data. All data were georeferenced using the WGS84 coordinate system, making the UAV system well-suited for water quality monitoring and analysis in complex aquaculture environments.

Data collection took place when the weather was clear and windless to ensure image quality. Flights were scheduled during two distinct time windows—9:00–10:00 AM and 3:00–4:00 PM—when the solar elevation angle is moderate and illumination is stable, thereby minimizing the risk of glare. The UAV was flown at an elevation of 150 meters, with a speed of 12 m/s during flight, achieving a high spatial resolution of 0.08 m × 0.08 m. The flight path overlap rate was set at 75% to ensure continuous image coverage, facilitating seamless mosaicking and subsequent analysis. Before each flight, the multispectral sensors on the UAV were calibrated using a standard white reference panel to correct for sensor response variability. The collected multispectral imagery was processed using Pix4D software for image mosaicking and radiometric calibration, resulting in five-band multispectral orthomosaics (as shown in Figure 2c). Multispectral data extraction and field sample analysis were performed using ENVI 5.3 software. For each sampling point, a region of interest (ROI) was delineated, centered on the sampling location, with a minimum area of 10 × 10 pixels to ensure the inclusion of a homogeneous water surface. The mean reflectance values for each spectral band within the ROI were calculated and used as the representative spectral signature of the sampling point. This approach enhances the representativeness of sampling data, reduces the influence of external environmental noise, and ensures the accuracy of reflectance extraction.

Equation 1 presents the radiation calibration formula:

$$\mathrm{R}_t = \frac{RAD_t * R_b}{RAD_b} \tag{1}$$

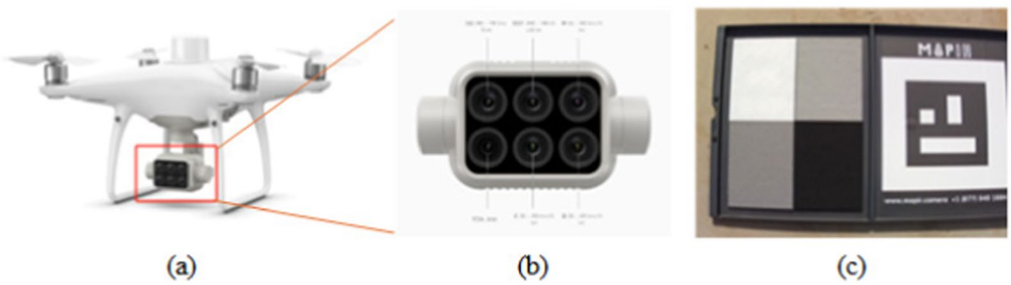

FIGURE 2
UAV and calibration plate. **(a)** DJI Phantom 4 multispectral drone. **(b)** Multispectral sensor lens. **(c)** Pix4D software.

TABLE 1 Spectral regions and wavelength ranges of Unmanned Aerial Vehicle (UAV) multispectral images.

Band	Wavelength range (nm)
Blue	450 ± 16
Green	560 ± 16
Red	650 ± 16
Red Edge	730 ± 16
Near IR	840 ± 26

In the formula, R_t is the spectral reflectance of the water body, R_b is the spectral reflectance of the calibration plate, RAD_t is the DN value of the measured water body, RAD_b is the DN value of the calibration plate.

2.3 Technological process

The methodology of this study involves the following essential procedures: (1) Collection and preprocessing of multispectral data from UAVs and in-situ water samples to ensure data quality; (2) Calibration of UAV Multispectral imagery and construction of spectral features based on both uncorrected and corrected data; (3) Spectral feature importance was assessed using Pearson correlation analysis and SHAP values, and the optimal subset of spectral features was selected for model training; (4) DOM estimation models were constructed using Light Gradient Boosting Machine (LightGBM), eXtreme Gradient Boosting (XGBoost), and Random Forest (RF) algorithms, followed by validation and testing. The accuracy comparison among the three models was used to verify the feasibility and effectiveness of the spectral correction method; (5) Based on both uncorrected and corrected data, a transfer learning approach was adopted. By incorporating cross-year data, the adaptability and generalization capability of the model were enhanced to ensure stability under different temporal and environmental conditions; (6) Using the optimal model, a full—scale estimation of DOM concentration within aquaculture ponds was achieved, and dynamic DOM concentration distribution diagrams were generated. The detailed technical workflow of this method is shown in Figure 3.

2.3.1 Water extraction

Water body extraction is a crucial step in water quality parameter detection. Accurately identifying and separating pure water areas provides reliable foundational data for estimating water quality. Within aquaculture ponds, aquatic vegetation contributes significantly to water quality improvement water quality, providing habitats for organisms and optimizing the ecological environment. Aquatic plants can absorb nutrients and some harmful substances from the water, increase the concentration of DOM, and provide food and shelter for aquatic animals such as the Chinese mitten crab. However, the presence of aquatic plants also affects the spectral reflectance characteristics of the water body, leading to spectral mixing, which increases the complexity of water quality parameter inversion. Therefore, accurately extracting the pure water area in ponds is crucial for water quality monitoring.

The Normalized Difference Water Index (NDWI) is a widely used indicator for water body information extraction. It is based on the strong absorption characteristics of water in the near-infrared (NIR) band and the strong reflection characteristics of vegetation in this band. NDWI effectively suppresses vegetation interference and highlights water body information, thus enabling precise extraction of water areas. This study utilizes the NDWI index to extract the water bodies in the study area, calculate the NDWI spatial distribution map of the ponds, and generate a histogram to analyze the distribution characteristics of NDWI values. Based on the histogram analysis results, the NDWI threshold range for pure water areas is determined to be [0.05, 0.2]. NDWI values exceeding this threshold represent pure water areas, while values below this threshold correspond to other non-water areas. The NDWI is calculated as shown in Equation 2:

$$\mathrm{NDWI} = \frac{\rho_G - \rho_{NIR}}{\rho_G + \rho_{NIR}} \tag{2}$$

In the formula, ρ_G denotes the green band reflectance of the multispectral data, ρ_{NIR} denotes the near-infrared band reflectance of the multispectral data.

2.3.2 Spectral correction method

The data in this study spans an extended period, covering different time points, seasons, and years. Due to variations in solar radiation intensity, solar zenith angle, and other lighting conditions at various time points, the spectral data from drone-based multispectral imagery is susceptible to the effects of lighting conditions, as shown in Figure 4. These lighting changes can result in differences in spectral reflectance for the same water body at different times, thus reducing the consistency between images from different time points. This, in turn, affects the applicability of cross-temporal data within the same model and weakens the model's stability and predictive accuracy.

To improve the consistency of multispectral data obtained at different times, this study proposes a spectral calibration method that focuses on the impact of variations in lighting intensity and solar zenith angle on water surface reflectance characteristics of ponds. This method combines the temporal variations of solar intensity and incident angle to calibrate the multispectral data from drones, reducing the spectral data deviations caused by time differences. It generates consistent and comparable spectral data across different time periods, providing a reliable data foundation for temporal change analysis and the estimation of DOM. The specific steps are outlined below.

Calculation of the sum of bands for each data point using Equation 3:

$$N_i = R_{i1} + R_{i2} + R_{i3} + R_{i4} + R_{i5} \tag{3}$$

Where R_{ij} represents the reflectance value of the i-th data point in the j-th band, and N_i is the total sum of the bands for the i-th data point.

Calculation of the correction coefficient via Equation 4:

$$C = \frac{1}{n}\sum_{i=1}^{n} N_i \tag{4}$$

Where C is the correction coefficient, reflecting the overall spectral reflectance level of the dataset. n is the total number of data points included in the calculation.

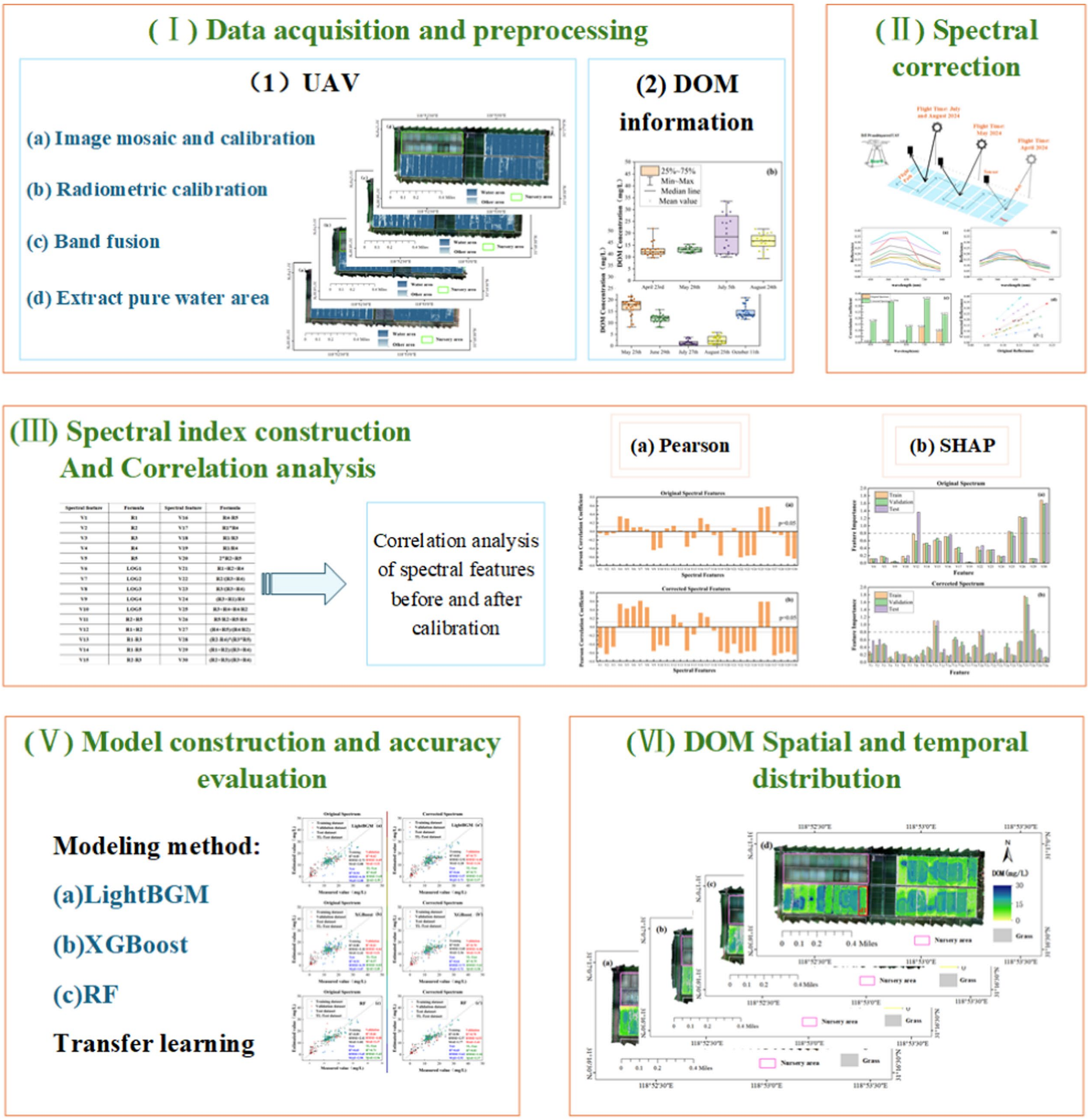

FIGURE 3
Technical flowchart.

Calculation of the corrected sum of bands in Equation 5:

$$N_i^{'} = \frac{N_i}{C} \tag{5}$$

Where $N_i^{'}$ is the corrected sum of bands for the i-th data point.
Error estimation in Equation 6:

$$N_i^{''} = round\left(N_i^{'}, 2\right) \tag{6}$$

Where $N_i^{''}$ represents the result of rounding $N_i^{'}$ to two decimal places.

Correction of band reflectance in Equation 7:

$$R_{ij}^{'} = \frac{R_{ij}}{N_i^{''}} \tag{7}$$

In the formula, $R_{ij}^{'}$ represents the reflectance value of the i-th data point in the j-th band after calibration. This calibration reduces the reflectance variations caused by different lighting intensities and solar zenith angles, ensuring consistency in multi-temporal data under varying lighting conditions and improving the accuracy and generalization ability of the model for multi-temporal estimations.

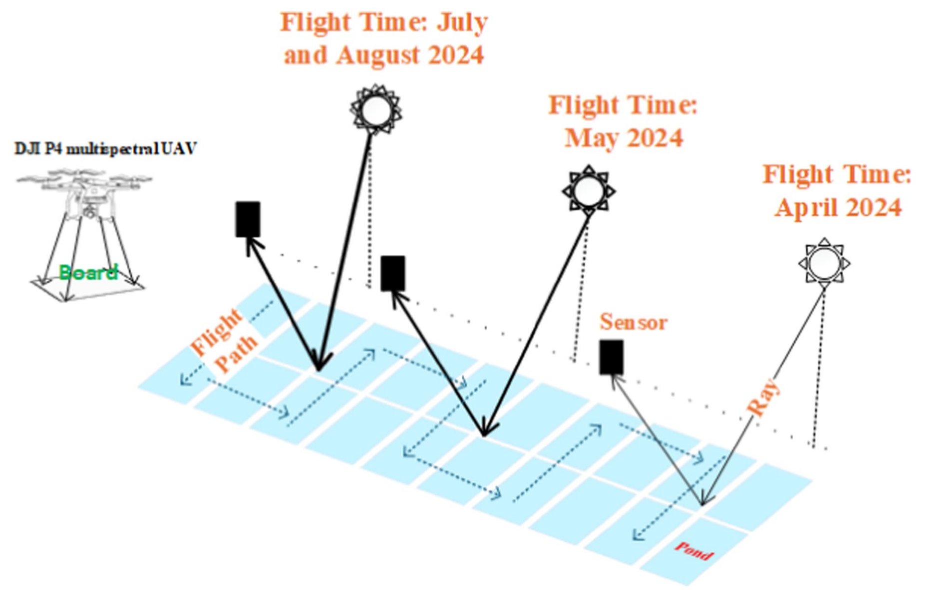

FIGURE 4
Variation of the illumination angle.

2.3.3 Spectral features extraction

Spectral features are important indicators for assessing water quality. By analyzing spectral features, we can directly understand the health status of water bodies. In this study, multispectral data obtained by drones were used to extract reflectance values from five bands: blue (B), green (G), red (R), red edge (Red Edge), and near-infrared (NIR) as the basic spectral features. These bands were combined and computed to construct multiple spectral features, enhancing the correlation of DOM in the spectral domain. Following previous studies (Zhang et al., 2021), this study performed a correlation analysis between the DOM index as well as the spectral reflectance at the points of sampling, selecting the DOM-sensitive bands and constructing 30 spectral features for subsequent selection and comparison. The specific spectral features are shown in Table 2.

2.3.4 Feature screening methods

Feature selection is a key step in improving model performance. By selecting the most relevant features from a large set, it is possible to effectively enhance model estimation accuracy, reduce computational complexity, avoid overfitting, and improve model interpretability.

Pearson correlation analysis is a commonly used statistical method for measuring the linear connection between two variables. The correlation coefficient spans from −1 to 1, with values close to ±1 indicating a strong linear relationship between the variables and values close to 0 indicating little to no correlation. By performing Pearson correlation analysis, we can identify spectral features that are significantly correlated with changes in DOM concentration. Strongly correlated features help improve model estimation accuracy. To further confirm the significant relationship between spectral features and DOM concentration, we used a significance test to select features that meet the significance level of $p < 0.05$ (Cleophas and Zwinderman, 2018).

TABLE 2 Spectral feature construction and calculation.

Spectral feature	Formula	Spectral feature	Formula
V1	R1	V16	R4-R5
V2	R2	V17	R1*R4
V3	R3	V18	R1/R3
V4	R4	V19	R1/R4
V5	R5	V20	2*R2 + R5
V6	LOGR1	V21	R1 + R2 + R4
V7	LOGR2	V22	R2/(R3 + R4)
V8	LOGR3	V23	R3/(R3 + R4)
V9	LOGR4	V24	(R3 + R1)/R4
V10	LOGR5	V25	R3 + R4 + R4/R2
V11	R2 + R5	V26	R5/R2 + R5/R4
V12	R1 + R2	V27	(R4 + R5)/(R4/R2)
V13	R1 − R3	V28	(R2-R4)*(R3*R5)
V14	R1 − R5	V29	(R1 + R2)/(R3 + R4)
V15	R2 − R3	V30	(R2 + R3)/(R3 + R4)

To comprehensively assess the contribution of each spectral feature to the estimation of DOM concentration, this study introduces the Shapley Additive explanation (SHAP) method for feature importance analysis. Compared to traditional feature evaluation methods, the SHAP method not only accurately quantifies the impact of each spectral feature on the model's estimation results but also effectively captures the marginal contribution of individual features and reveals interactions between features. The SHAP values are computed by considering all possible feature combinations, thus avoiding the biases that may arise from evaluating a single feature in isolation, providing a more comprehensive and accurate feature importance metric, and enhancing model interpretability (Yao et al., 2025). In SHAP analysis, features with high SHAP values have a positive contribution to the estimation results, while features with low SHAP values negatively impact the estimation. For tree-based models, SHAP values are computed using the Tree SHAP algorithm, which optimizes the computation of feature contributions for each path, improving computational efficiency. Given a tree T, the Shapley value for each node can be represented by the path contribution formula in Equation 8:

$$\phi_j(f) = \sum_{path_p} \frac{p(path_p)}{p_{total}} \cdot \Delta_j(path_p) \tag{8}$$

Where $p(path_p)$ represents the weight of path p, typically related to the frequency of its occurrence; p_{total} denotes the total number of paths; and $\Delta_j(path_p)$ indicates the marginal contribution of feature j to the estimation along path p.

2.3.5 Modeling methodology

This study uses LightGBM, XGBoost, and RF algorithms to estimate the concentration of DOM and introduces the transfer learning approach to enhance the model's generalization ability over time. Additionally, a data correction method is applied to improve the model's stability and robustness.

Based on gradient boosting decision trees, LightGBM is a highly efficient machine—learning algorithm, known for its excellent computational performance and strong generalization capabilities. The algorithm uses the best split method based on leaves and data histogram optimization techniques to improve the efficiency of large-scale data processing, and simultaneously demonstrates strong capabilities in handling high-dimensional sparse data. Unlike the traditional "breadth-first" approach, LightGBM adopts a "depth-first" strategy, making it more efficient when handling large datasets. Additionally, LightGBM can directly process categorical features without requiring one-hot encoding, reducing the complexity of data preprocessing. By performing balanced splits at each leaf node of the tree, the model can better capture the nonlinear relationships within the data, further enhancing estimation accuracy.

XGBoost is an efficient, flexible, and scalable machine learning algorithm. Integrating multiple weak learners progressively reduces estimation errors and utilizes gradient information to fit the residuals from the previous round. This allows it to effectively handle complex data and the relationships between nonlinear features. Compared to traditional Gradient Boosting Decision Tree (GBDT), XGBoost has made several optimizations, such as incorporating both first- and second-order gradient information to stabilize the optimization process. It also uses L1 and L2 regularization to control model complexity and prevent overfitting. Moreover, XGBoost supports column sampling, automatic handling of missing values, parallelized computation, and distributed training, thereby improving its computational efficiency and robustness in large-scale data processing. Its cache-aware data structure further optimizes memory usage, making it particularly well-suited for high-dimensional sparse data. XGBoost also supports custom objective functions and evaluation metrics, and its early stopping strategy ends the training when there is no further enhancement in the validation set performance, thus saving computation costs and enhancing generalization ability.

RF is a supervised learning algorithm based on ensemble learning, which improves estimation accuracy and stability by integrating multiple decision tree models. Its core concept involves constructing several weak learners and aggregating their outputs through classification or regression strategies. In contrast to a single decision tree, RF has multiple benefits. By combining multiple decision trees, RF effectively mitigates overfitting risk and improves model generalization. Additionally, since each decision tree is trained independently, RF supports efficient parallel computation.

Transfer learning, as a cross-domain knowledge transfer approach, enables the application of knowledge acquired from existing tasks to the acquisition of new tasks (Lumini and Nanni, 2019). By leveraging knowledge gained from related tasks in the source domain, it enhances the learning capability of new tasks in the target domain (Weber et al., 2021). Model-based transfer learning involves using pre-trained machine learning models trained on large-scale data from the source domain and then adapting these models to the target domain through fine-tuning with limited target data to achieve localized optimization and adaptation (Zhuang et al., 2021). Fine-tuning is a common strategy in transfer learning, wherein the pre-trained model is further trained to accommodate new tasks or datasets. During this process, the feature representations learned from the source task are typically retained, while only a portion of the model parameters, particularly those in the final layers, are adjusted. Fine-tuning not only improves the model's ability to adapt to the target task through parameter adjustment but also leverages the relevant information already acquired in the source task, thereby accelerating convergence and enhancing estimation accuracy.

2.3.6 Accuracy verification

This study, model training and validation were conducted using the 2023 dataset, while the 2024 dataset was employed to test the temporal generalization capability of the model. To comprehensively evaluate the predictive performance of the model, multiple accuracy assessment metrics were adopted, comprising Root Mean Square Error (RMSE), Coefficient of Determination (R^2), and Mean Absolute Error (MAE).

RMSE serves to gage the disparity between predicted and actual values and serves as a common metric for assessing the predictive accuracy of regression models. It provides an intuitive measure of the magnitude of estimation errors—a lower RMSE indicates a better model fit and higher predictive capability. R^2 measures the degree to which the model accounts for data variance. With a scale from 0 to 1, values approaching 1 suggest higher explanatory power. In model validation and testing, a high R^2 value suggests that the model effectively captures the variation trends in the data and demonstrates strong predictive performance. MAE, another error metric, is the mean of the absolute differences of predicted and actual values. MAE exhibits lower sensitivity to outliers and provides a straightforward reflection of the model's estimation error.

The specific formulas for calculating R^2, RMSE, and MAE are given in Equations 9–11:

$$\mathrm{R}^2 = 1 - \frac{\sum(y_i - \hat{y}_i)^2}{\sum(y_i - \bar{y}_i)^2} \tag{9}$$

$$\mathrm{RMSE}=\sqrt{\frac{1}{n}\sum_{i=1}^{n}\left(\hat{y}_i-y_i\right)}^{2} \tag{10}$$

$$\mathrm{MAE}=\frac{1}{n}\sum_{i=1}^{n}\left|\hat{y}_i-y_i\right| \tag{11}$$

In the above formulas, $\hat{y}_i$represents the predicted value of the water quality parameter, y_i represents the measured value of the water quality parameter, $\overline{y}_i$ represents the mean of the measured values of the water quality parameter, n is the number of sampling points.

3 Results

This section may be divided by subheadings. It should provide a concise and precise description of the experimental results, their interpretation, as well as the experimental conclusions that can be drawn.

3.1 Statistical analysis of samples

Figure 5 shows the distribution of DOM concentration for the sampling months of 2023 and 2024. Specifically, Figure 5a illustrates the DOM concentration distribution for April, May, July, August, and October of 2023, while Figure 5b displays the DOM concentration distribution for April, May, July, and August of 2024.

3.2 Water extraction

The value of the NDWI typically ranges from −1 to 1, with values less than 0 usually corresponding to non-water areas. However, the NDWI value is influenced by various factors, meaning that the threshold for distinguishing water and non-water areas is not fixed and needs to be adjusted based on the study area and imagery data. In this study, we first used UAV multispectral data to generate NDWI images for the study area. Through histogram distribution and visual interpretation, we determined the optimal threshold for water extraction in this research area. After analysis, we selected an NDWI threshold range of [0.05, 0.2]. Based on this threshold, we performed binary processing of the UAV multispectral images. When the NDWI value exceeded the threshold, it was classified as a water area; when the NDWI value was less than or equal to the threshold, it was marked as other areas. Figure 6 shows the water extraction images for the aquaculture base, where Figures 6a–d represent the water extraction results for April, May, July, and August 2024, respectively.

3.3 Spectral correction analysis

Figure 7 shows the multispectral curves of the water body before and after correction, along with their respective coefficients of determination when compared to DOM concentration. Figure 7a presents the multispectral reflectance curve of the water body before correction, while Figure 7b shows the multispectral reflectance curve after correction. Figure 7c displays a histogram of the coefficients of determination between each band and DOM concentration before and after spectral correction, and Figure 7d illustrates the correlation of spectral reflectance for each band before and after correction. From Figures 7a,b, it can be seen that before correction, the water body's spectral reflectance exhibits an overall lifting or lowering phenomenon, which is primarily caused by variations in light intensity. This phenomenon significantly interferes with the sensitivity of the spectral data to changes in DOM concentration. After correction, the water body's reflectance spectra become consistent, with no overall increase or decrease, thereby effectively correcting the impact of light intensity variation on the spectral data. As shown in Figure 7c, prior to correction, the correlation between the spectral data and DOM concentration was extremely low due to the influence of solar intensity differences. After correction, the correlation between the spectral data and DOM concentration is significantly improved, indicating that the proposed spectral correction method effectively enhances the sensitivity of the spectral data to DOM concentration. Figure 7d shows that the correlation coefficients of the reflectance of each band before and after correction are all 1, demonstrates that the spectral data after correction shows complete consistency with the original spectral data, and no information has been lost.

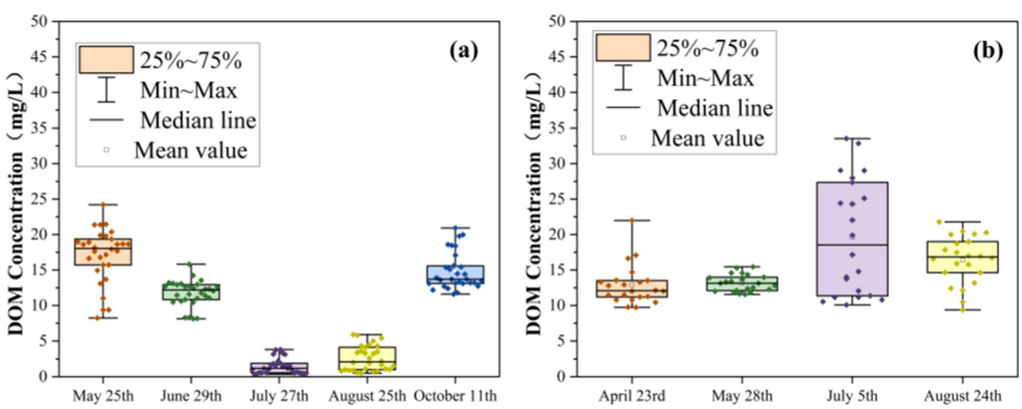

FIGURE 5
Statistical distribution of dissolved organic matter (DOM) concentration data. **(a)** DOM concentration distribution in April, May, July, August, and October 2023. **(b)** DOM concentration distribution in April, May, July, and August 2024.

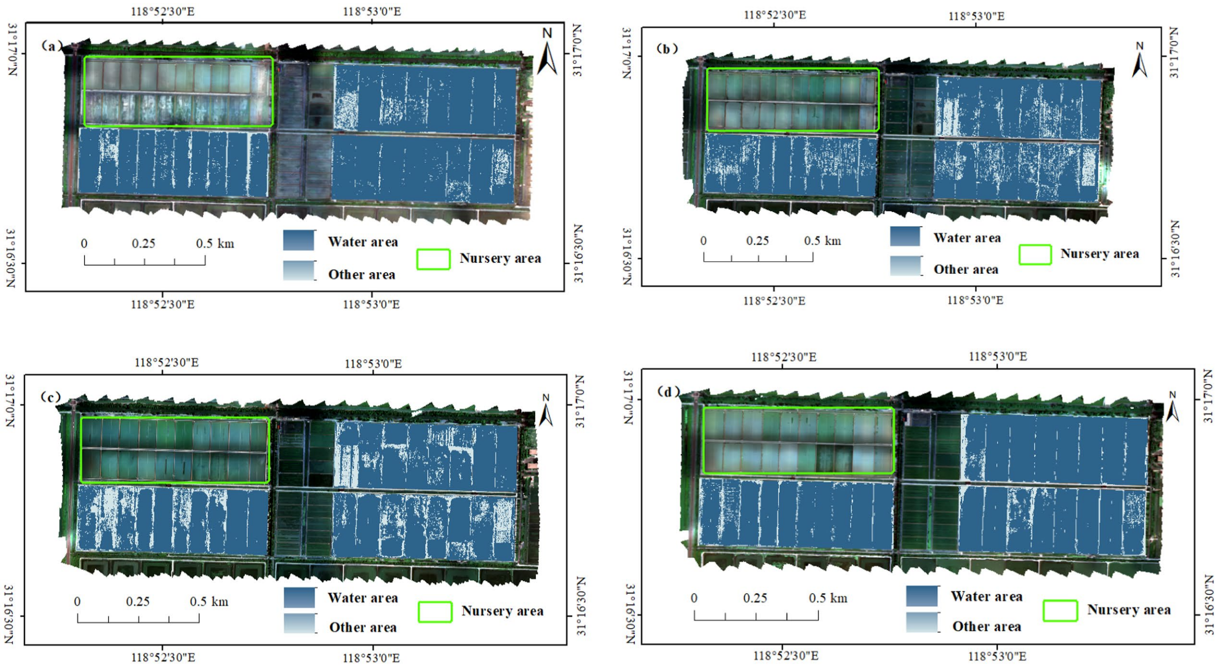

FIGURE 6
Extracted images of pond waters at the farm base. **(a)** April farm base waters image; **(b)** May farm base waters image; **(c)** July farm base waters image; **(d)** August farm base waters image.

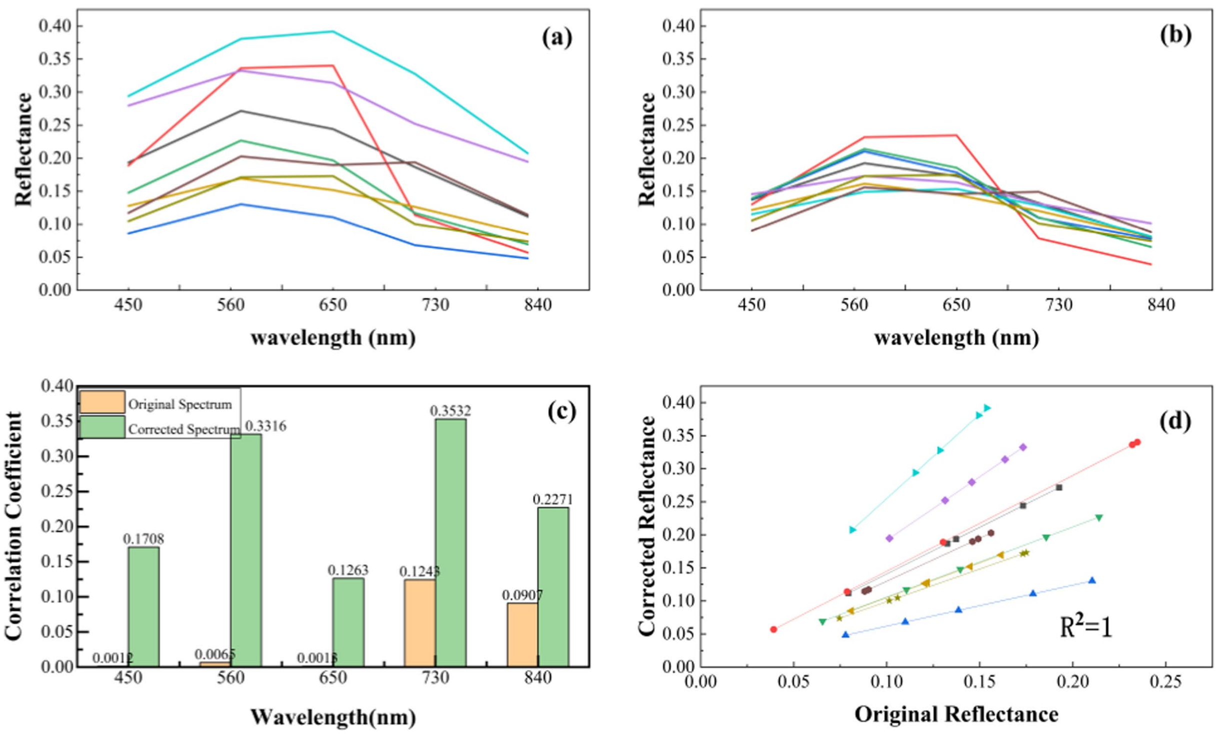

FIGURE 7
(a) Reflectance of the same pond at different times before correction; **(b)** Reflectance of the same pond at different times after correction; **(c)** Correlation between DOM concentration and spectral data before and after correction; **(d)** Correlation of spectral reflectance at each band between pre- and post-correction samples.

3.4 Correlation analysis between DOM concentration and spectral characteristics

To comprehensively analyze the relationship between spectral features and DOM concentration before and after spectral correction, this study employed Pearson correlation analysis on 30 spectral features. Spectral features that were statistically significant with a significance level of $p < 0.05$ were selected for further analysis.

Figure 8 presents the Pearson correlation analysis results between spectral features and DOM concentration. Figure 8a shows the results based on the original spectral data, and Figure 8b shows the results after spectral correction. By comparing Figures 8a,b, it can be observed that, in terms of correlation direction, most spectral features maintained consistent relationships with DOM concentration before and after correction. It shows that the spectral correction method applied in this research effectively preserved the original correlation trends between the spectral data and DOM concentration. Among the spectral features V1–V30, V11, V20, and V21 exhibited changes in correlation direction with DOM concentration after correction. However, the absolute magnitudes of their correlation coefficients were all below 0.10, suggesting that these features had very weak correlations and could not reliably represent the underlying relationship between spectral characteristics and DOM concentration. In terms of correlation strength, the spectral features derived from the corrected spectra showed significantly stronger correlations with DOM concentration compared to those from the original spectra, with the average absolute value of the correlation coefficients increasing by 465.02%. These results demonstrate that the spectral correction method presented herein effectively enhances the sensitivity of spectral features to DOM concentration.

Figure 9 illustrates the SHAP value analysis results between spectral features and DOM concentration. Figure 9a shows the SHAP values based on the original spectral data, and Figure 9b presents the SHAP values based on the corrected spectral data. As shown in Figure 9a, among the 17 spectral features with $p < 0.05$ selected through Pearson correlation analysis, V12, V25, V26, and V30 exhibited mean absolute SHAP values greater than 0.8, which shows that these features had a significant impact on the model's estimations. According to the SHAP values derived from the corrected spectral data in Figure 9b, among the 28 spectral features with $p < 0.05$ identified through Pearson correlation analysis, V11, V20, V27, and V28 showed relatively high mean absolute SHAP values, all exceeding 0.8. Notably, V20, V27, and V28 not only demonstrated statistical significance in the Pearson correlation analysis but also exhibited high importance in the SHAP analysis.

Therefore, based on a comprehensive evaluation combining Pearson correlation analysis and SHAP feature importance assessment, four spectral features with mean absolute SHAP values greater than 0.8 served as the input variables for the model. Through the integrated assessment of both analytical methods, the selected spectral features were demonstrated to effectively capture the variation trends of DOM concentration and serve as important input variables for model

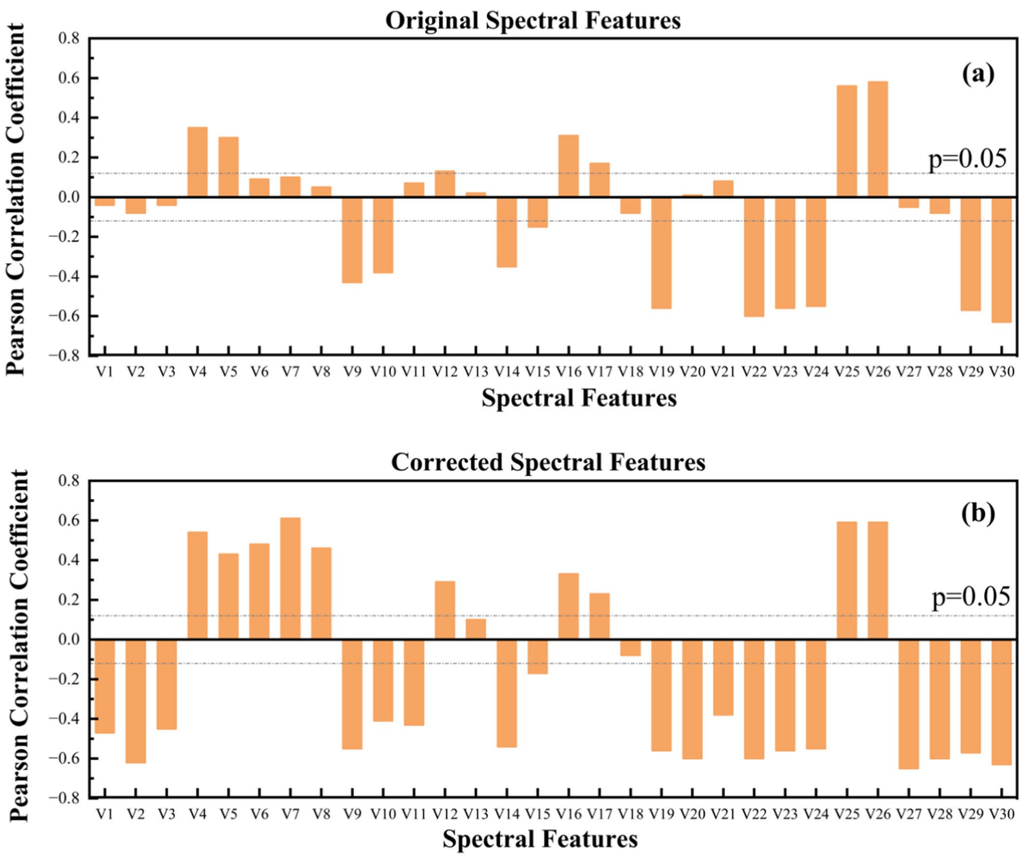

FIGURE 8
Chart of Pearson correlation analysis between spectral features and DOM concentration. **(a)** Chart of Pearson correlation coefficients based on the original spectral features; **(b)** Chart of Pearson correlation coefficients based on the corrected spectral features.

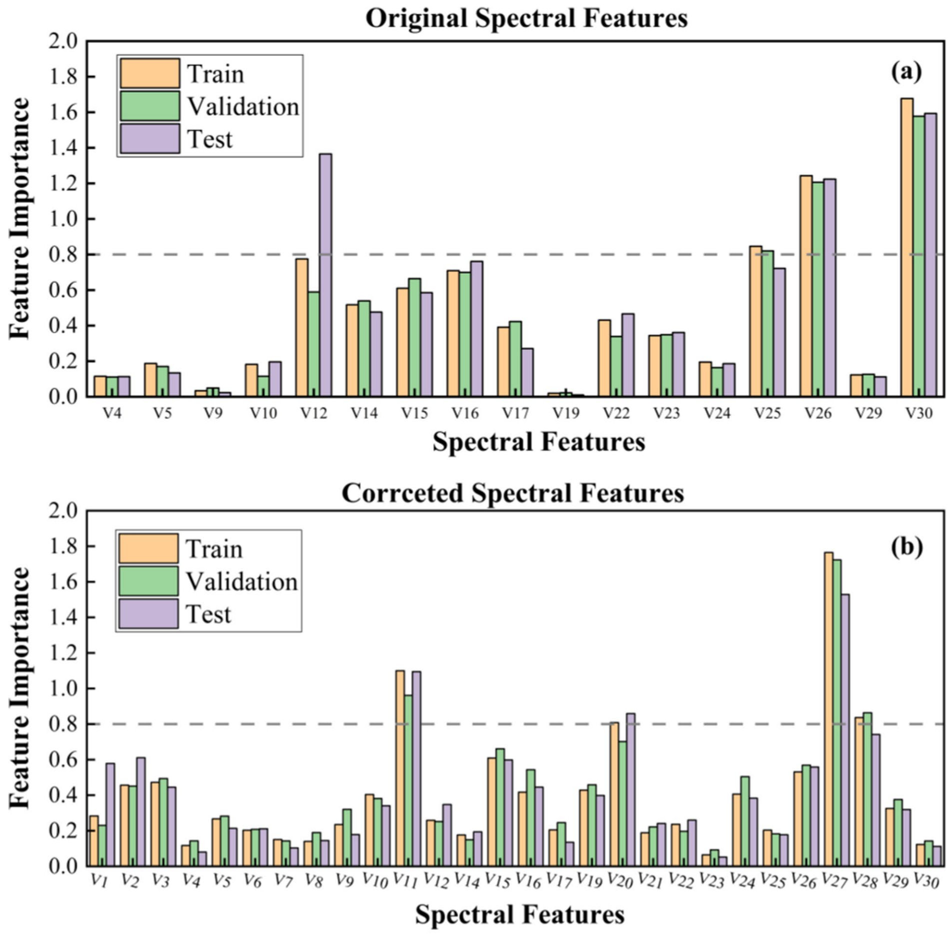

FIGURE 9
Chart of SHAP value analysis for spectral features before and after correction. **(a)** SHAP values based on the original spectral features; **(b)** SHAP values based on the corrected spectral features.

TABLE 3 Accuracy evaluation of DOM concentration estimation models.

Base	Model	Training			Validation			Test			TL-Test		
		R^2	RMSE	MAE	R^2	RMSE	MAE	R^2	RMSE	MAE	R^2	RMSE	MAE
Original	LightBGM	0.85	2.73	2.08	0.62	4.69	3.53	0.54	4.2	2.88	0.65	3.69	2.59
	XGBoost	0.80	3.18	2.42	0.62	4.64	3.51	0.51	4.39	3.07	0.57	4.03	2.85
	RF	0.89	2.41	1.82	0.66	4.68	3.37	0.65	3.65	2.58	0.71	3.43	2.56
Corrceted	LightBGM	0.83	2.92	2.28	0.73	4.4	3.34	0.66	3.57	2.71	0.71	3.43	2.57
	XGBoost	0.81	3.05	2.36	0.7	4.4	3.35	0.64	3.73	2.72	0.69	3.61	2.58
	RF	0.9	2.37	1.77	0.7	4.53	3.41	0.65	3.62	2.52	0.82	3.1	2.37

optimization, providing a reliable foundation for the subsequent development of a high-efficiency and stable DOM concentration estimation model.

3.5 DOM model performance analysis

Table 3 presents the modeling results for DOM concentration estimation. In the table, "Training" refers to the training dataset (2023), "Validation" refers to the validation dataset (2023), "Test" represents the model evaluation using field measurements from 2024, and "TL-Test" refers to the testing results on the 2024 field measurements after incorporating the transfer learning approach. The modeling effects of three machine learning models (LightGBM, XGBoost, and RF) on DOM concentrations are summarized before correction, after spectral correction, and after applying the transfer learning approach. Figure 10 illustrates the correspondence between observed and predicted DOM concentrations for the three machine learning models.

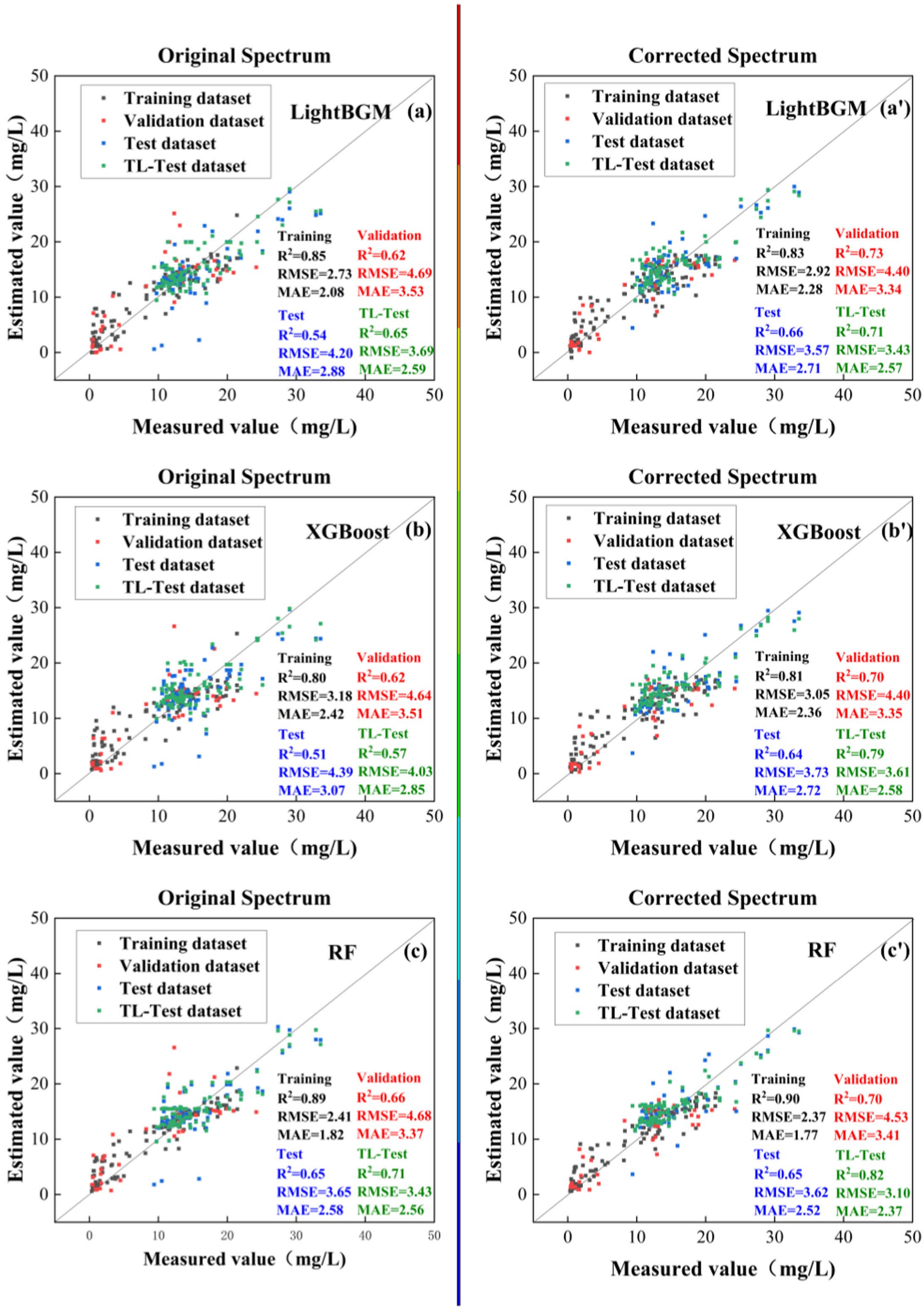

FIGURE 10
Scatter plots of DOM concentration estimation by machine learning models. **(a)** Scatter plot of measured samples and LightGBM-estimated values before spectral correction. **(a′)** Scatter plot of measured samples and LightGBM-estimated values after spectral correction. **(b)** Scatter plot of measured samples and XGBoost-estimated values before spectral correction. **(b′)** Scatter plot of measured samples and XGBoost-estimated values after spectral correction. **(c)** Scatter plot of measured samples and RF-estimated values before spectral correction. **(c′)** Scatter plot of measured samples and RF-estimated values after spectral correction.

As shown in Table 3, a comparative study of the indicators for the Training, Validation, and Test sets reveals that the spectral correction significantly improved the estimation accuracy across different machine learning models compared to using raw spectra, particularly by reducing errors and enhancing model fitting ability. Based on the 2023 validation dataset results, spectral correction led to improvements in R^2 for all models. Specifically, LightGBM achieved an 18% increase in R^2, with RMSE and MAE reductions of 6 and 5%, respectively; XGBoost

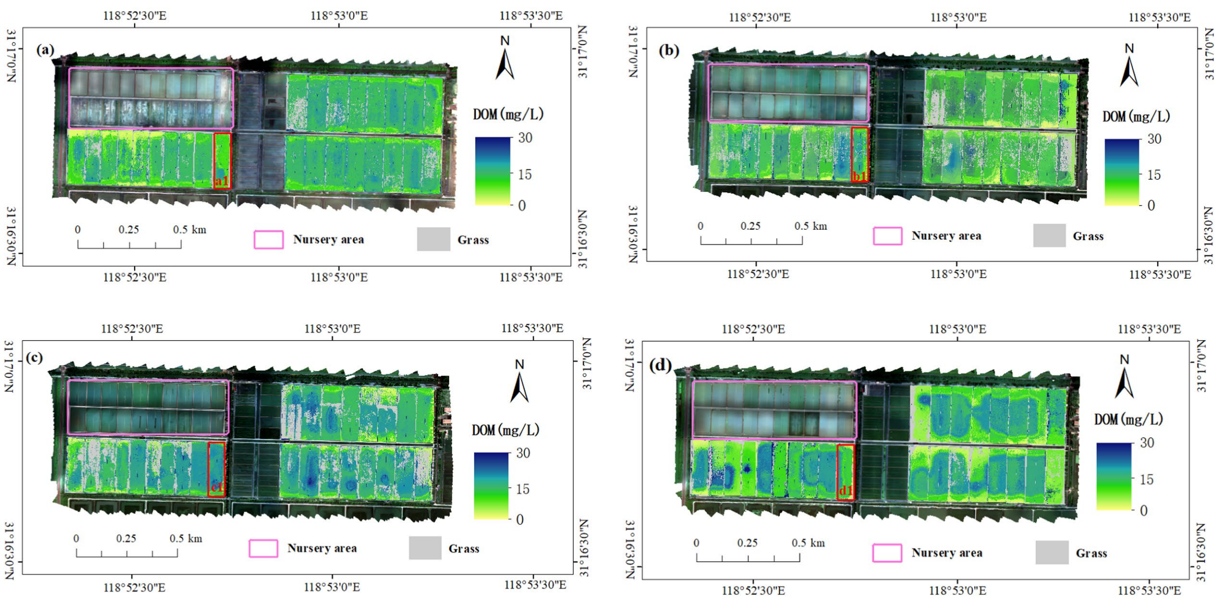

FIGURE 11
Spatial distribution maps of DOM concentrations. **(a)** April 2024; **(b)** May 2024; **(c)** July 2024; **(d)** August 2024.

showed a 13% increase in R^2, with 5% reductions in both RMSE and MAE; RF demonstrated a 6% improvement in R^2. Analysis of the Test set indicates that the R^2 values for the LightGBM and XGBoost models increased by 22 and 25%, respectively, with RMSE reductions of 15% and MAE reductions of 6 and 11%, respectively. The RF model also showed notable improvements, indicating that spectral correction significantly enhanced the estimation performance on the test dataset.

A comparison between the Transfer Learning-Test (TL-Test) and Test results further demonstrates that the use of the transfer learning approach enhanced the models' generalization ability on the 2024 test data. Compared with models without fine-tuning, models adjusted through the transfer learning approach exhibited markedly improved performance. Without spectral correction, the transfer learning approach resulted in a 20% increase in R^2 for the LightGBM model, with RMSE and MAE reductions of 12 and 10%, respectively. The R^2 values for XGBoost and RF improved by 12 and 9%, respectively, with corresponding reductions in RMSE and MAE. After applying the transfer learning approach following spectral correction, the RF model achieved a 26% improvement in R^2 on the test set compared to the RF model using only spectral correction, with reductions of 14 and 6% in RMSE and MAE, respectively. The LightGBM and XGBoost models also exhibited an 8% increase in R^2 after the transfer learning approach. These results demonstrate that the transfer learning approach, when combined with spectral correction, further enhances the models' adaptability to temporal and environmental variations.

The analysis of the TL-Test reveals that the combined use of spectral correction and the transfer learning approach significantly enhanced the overall performance of the LightGBM, XGBoost, and RF models. Specifically, R^2 increased by 31, 35, and 26%, respectively, while RMSE decreased by 18, 18, and 15%, and MAE decreased by 11, 16, and 8%. From spectral correction to the transfer learning fine-tuning process, "model performance improved steadily throughout the process. Spectral correction effectively enhanced the correlation between spectral features and DOM concentration, optimizing input variables and enhancing both the exactness and steadiness of the model. The transfer learning approach further mitigated the impact of cross-year data distribution differences on model performance, achieving optimal estimation accuracy on the test set. Notably, the RF model demonstrated outstanding performance after the transfer learning approach, with an R^2 value reaching 0.82, confirming its advantage in DOM concentration modeling. Therefore, the combined use of spectral correction and the transfer learning approach significantly improves the accuracy and stability of DOM estimation, particularly exhibiting stronger adaptability in cross-year modeling scenarios.

3.6 DOM spatial distribution map

Based on the UAV multispectral imagery of pure water areas obtained after the identification and exclusion of aquatic plants, sensitive spectral index values were calculated for each pixel. These values were then input into the previously established optimal model for DOM concentration estimation, enabling the generation of DOM concentration estimates at the pixel level. Consequently, spatial distribution maps of DOM concentrations across the aquaculture ponds were produced. Figure 11 presents the spatial distributions of DOM concentrations in April, May, July, and August 2024.

Table 4 presents the average values of DOM concentrations obtained from field measurements and model estimations, as well as the average temperatures over the 5 days preceding the sampling dates in April, May, July, and August 2024. A comparison of the data revealed that the predicted and observed values exhibited generally consistent trends, effectively capturing the seasonal variation characteristics of DOM concentrations. However, some discrepancies between the predicted and measured values are observed across different months: the predicted values for July and August are slightly inferior to the measured values, while those for April and May are somewhat superior. The overall small errors between the estimation and the measurements indicate that the constructed model can accurately estimate the variations in DOM concentrations.

TABLE 4 Mean values of measured and estimated DOM concentrations and the average experimental air temperature.

Indicator	April	May	July	August
Measured average (mg/L)	12.86	13.17	19.66	16.42
Predicted average(mg/L)	13.41	13.64	18.86	15.52
Average temperature (5 days before the experiment) (°C)	22.6	29.2	34.0	33.4

Analysis of the spatial distribution presented in Figure 11 indicates that the concentration of DOM in the pond water showed an overall increasing trend from April to July, followed by a slight decrease in August. This pattern can be primarily attributed to the significant influence of temperature on DOM concentrations, with higher temperatures promoting an increase in DOM levels. In addition, precipitation exerts a dilution effect on DOM concentrations. Based on meteorological observation data from the Gaochun region, the temperature gradually increased from April to July, while it slightly decreased in August. Additionally, the region was influenced by an upper-level trough, and strong rainfall occurred before the experiment in August, with a cumulative rainfall of 75.4 mm. From a spatial perspective, DOM concentration exhibited pronounced spatial heterogeneity, with lower concentrations observed near the pond banks. In freshwater aquaculture ponds, DOM primarily originates from the metabolic products of cultured organisms, algae, and microbial activities, the input of feed and fertilizers, and external water inputs. The water depth in the pond gradually increases from the edges to the center, with shallower depths near the shore and deeper areas in the center. Due to the shallower depth near the bank, sedimentation is more pronounced, causing some organic matter to be more readily deposited or degraded by microorganisms, leading to relatively lower DOM concentrations. In contrast, the central region of the pond contains higher organic content in the sediment, and the water is more susceptible to disturbances from wind, boat movement, etc., which enhances water mixing, making DOM more likely to accumulate and result in higher concentrations. Aquaculture activities also influence the spatial distribution of DOM, as feed is typically concentrated in the central or designated feeding areas of the pond, which may lead to further increases in DOM concentrations in these regions. This spatial heterogeneity has important implications for pond water quality management.

4 Discussion

4.1 The application of remote sensing technology by UAV for water quality monitoring

Satellite remote sensing platforms for surface water monitoring have predominantly focused on large lakes or coastal aquaculture areas (Ottinger et al., 2022; Alparslan et al., 2009), whereas this study targets small inland freshwater ponds. Compared to monitoring natural lakes and coastal waters, inland freshwater ponds are characterized by smaller surface areas, shallower depths, higher aquatic vegetation coverage, greater anthropogenic disturbances, and faster and more complex spatiotemporal variations in water quality. These factors make it challenging to achieve high-resolution water quality monitoring using satellite remote sensing platforms (Wu et al., 2021; Peng and Chen, 2024). The UAV-based remote sensing platform exhibits a unique advantage of high spatial resolution in monitoring inland pond water information, providing essential data support for the monitoring of small water bodies. During this research, multispectral images featuring a spatial resolution of 8 cm were obtained via a UAV platform over the experimental area, effectively separating water body information within the ponds and laying a critical foundation for water quality monitoring, which is consistent with previous research findings (Sibanda et al., 2021).

Due to the complex optical properties of waterbodies and the extended temporal span of the data used in this study, UAV multispectral imagery was subject to multiple factors of interference. Previous studies primarily utilized UAV multispectral data combined with machine learning algorithms for modeling without considering the influence of other factors, thereby limiting the temporal applicability of the models (Wang et al., 2020). In this study, the spectral correction method was employed to integrate multi-temporal imagery data, effectively mitigating the impact of illumination variability on the consistency of remote sensing data. In addition, the transfer learning approach was incorporated for DOM concentration estimation. Experimental results demonstrated that the spectral correction method proposed in this study effectively enhanced the consistency of imagery acquired across different time periods. Combined with a transfer learning approach, it significantly improved the estimation accuracy of DOM concentrations, achieving the best model performance with an R^2 of 0.82 and an RMSE of 3.1 mg/L. Compared with similar studies, the estimation accuracy achieved in this study was notably higher, providing a technical framework for real-time aquatic quality monitoring and precision management in complex aquaculture environments.

4.2 The performance of spectral correction methods in water quality estimation

In aquaculture pond water quality monitoring based on UAV multispectral data, the variation of illumination conditions over time can cause abnormal fluctuations in the reflectance values of UAV multispectral images, resulting in spectral inconsistencies among images acquired at different times and subsequently affecting the estimation accuracy of DOM concentrations. In this study, the spectral correction method was applied to multispectral images acquired at multiple time points by UAVs, adjusting image data obtained under varying solar irradiance and solar elevation angle conditions to a unified standard, and thereby constructing a cross-temporal estimation model for DOM concentration. Compared with the calibration method based on the EVA grayscale reference panel (Jeong et al., 2018), this study proposed a spectral correction method to effectively address the issue of correcting the UAV image data across different time periods, expanding the applicability of the correction algorithm over the temporal dimension. Compared with methods that calibrate spectral data by observing various solar radiation parameters, the spectral correction method put forward in this research requires fewer parameters, is easier to operate, and demonstrates strong practicality, facilitating its application across different temporal scales (Singh and Nansen, 2017).

Experimental results showed that the Pearson correlation between the corrected spectral features and DOM concentration improved by an average of 465.02%. Prior to the application of the transfer learning approach, compared with the original spectral data, the validation R^2 of the model constructed using the corrected spectra increased by an average of 13.1%, while RMSE decreased by 10.0% and MAE decreased by 6.3%. Compared with other methods, the spectral correction method proposed in this study demonstrated superior performance in enhancing spectral sensitivity and estimation accuracy. Moreover, the proposed spectral correction method not only improved the consistency of imagery data across different temporal scales but also exhibited strong applicability under multi-temporal conditions, providing better support for long-term water quality monitoring and estimation in aquaculture ponds.

4.3 The performance of the transfer learning approach in DOM estimation

The limited spatiotemporal scalability of surface parameter estimation models is a common challenge currently faced in remote sensing applications. As an effective approach to enhance model generalization and address heterogeneous data distribution, transfer learning has become an important strategy for improving the spatiotemporal generalization capability of water quality estimation models. In this study, we estimated DOM concentration in freshwater aquaculture ponds using experimental data collected at different time periods. Due to environmental variations across different periods, discrepancies existed between datasets, necessitating the use of the transfer learning approach to optimize the models and reduce the impact of data variability on estimation results. Compared with previous studies, this research applied the transfer learning approach to models constructed from water sample data collected during different periods, thereby improving the cross-temporal adaptability and predictive accuracy of water quality parameter estimation models. Experimental results showed that the transfer learning approach effectively enhanced the model's adaptability to data from different time periods, consistent with previous findings (Fu et al., 2023; Chen X. et al., 2024; Zhang et al., 2024). The incorporation of a transfer learning approach significantly improved the generalization ability and estimation accuracy of models based on LightGBM, XGBoost, and RF algorithms.

Moreover, this study combined spectral correction methods with the transfer learning approach. Experiments demonstrated that the synergy between spectral correction methods and the transfer learning approach can effectively enhance the spatiotemporal generalization capability of the models and improve the accuracy of DOM concentration estimation. These findings may also provide a reference for the integration of other algorithms with transfer learning approaches.

4.4 Shortcomings and prospects

Due to the influence of climatic, geographical, and other environmental factors, variations in illumination conditions occur across different regions. The development and optimization of spectral correction methods can effectively enhance the spatiotemporal adaptability of remote sensing-based estimation models and remains one of the key challenges in remote sensing applications. This study proposes a UAV-based multispectral remote sensing method for water quality parameter estimation, which enhances the temporal adaptability of the model by leveraging spectral correction and the transfer learning approach. Although the study has achieved certain research outcomes through extensive experimental analysis, several limitations remain, requiring further investigation: (1) The effectiveness of the spectral correction method for cross-site and cross-temporal data remains unverified. This study was based on data collected from the same experimental site at different times. Whether the conclusions are applicable to different locations and larger temporal scales requires further validation. (2) The effectiveness for other types of remote sensing data remains unverified. The current study focused exclusively on UAV multispectral data. The applicability of the proposed spectral correction method for other types of remote sensing data still needs to be explored. (3) Further optimization of the spectral correction method. Although the experimental outcomes demonstrate that the put-forward spectral correction method is effective and feasible, improving spectral sensitivity to water quality parameters remains relatively limited. Whether further optimization of the spectral correction method can enhance the correlation between spectral data and water quality parameters still requires further experimentation to validate. Moreover, while this study improved the model's adaptability to 2024 data through spectral correction and the transfer learning approach, its generalization ability over longer time spans or across different regions still requires further validation.

5 Conclusion

This study proposes a spectral data correction method to resolve spectral variations arising from differences in observational conditions, such as solar altitude angle and light intensity, in UAV multispectral data collected at different times. Using pre- and post-correction spectral data, combined with feature parameter construction, sensitive feature selection methods, and the transfer learning approach, an estimation model for DOM concentration in water bodies was developed to validate the viability of the spectral correction approach. The research findings are as follows: (1) The proposed spectral correction method effectively adjusted water body spectral data from freshwater aquaculture ponds and significantly enhanced spectral sensitivity to DOM. (2) The correction method effectively mitigated the influence of outliers, improved model estimation accuracy, and enhanced temporal generalization capability. The integration of the spectral correction method with the transfer learning approach further improved both estimation accuracy and temporal generalization performance. (3) The spatial distribution map of DOM concentrations in freshwater aquaculture ponds, generated by the optimized model, aligns with the actual conditions of the experimental site. This demonstrates that the combination of the spectral correction method and the transfer learning approach enables accurate monitoring of DOM concentrations in freshwater aquaculture ponds, thereby supporting water quality management in such environments. (4) With the widespread adoption of UAV platforms and multispectral sensors in aquaculture, the spectral correction and cross-temporal modeling approach proposed in this study can be further extended to predict DOM concentrations across multiple time periods. This significantly reduces the frequency and labor intensity of traditional field sampling, enabling cost-effective, high-frequency water quality monitoring. (5) Leveraging the flexible deployment capability of UAVs and the efficient data acquisition of multispectral sensors, the proposed method can be seamlessly integrated into existing aquaculture operations for standardized implementation. By incorporating spectral correction and DOM estimation models into monitoring systems, the approach replaces conventional manual sampling procedures while enabling rapid analysis. Furthermore, centralized processing and remote prediction capabilities make this method adaptable to diverse aquaculture operations of varying types and scales. (6) The application of this method will substantially advance the practice of "remote sensing-based ecological aquaculture." Through continuous monitoring and dynamic analysis of key water quality parameters such as DOM, aquaculture managers can achieve precision feeding, scientific water regulation, and effective control of pollutant discharge. This contributes to enhanced production yields, improved environmental sustainability, and ultimately promotes the development of modern aquaculture systems characterized by green practices, ecological balance, and high efficiency.

Data availability statement

The original contributions presented in the study are included in the article/Supplementary material, further inquiries can be directed to the corresponding author.

Author contributions

WL: Writing – original draft, Validation, Visualization, Methodology, Conceptualization, Writing – review & editing. YW: Methodology, Conceptualization, Writing – review & editing, Funding acquisition, Resources. HC: Formal analysis, Data curation, Validation, Writing – review & editing. PC: Validation, Supervision, Writing – review & editing, Formal analysis. XG: Project administration, Writing – review & editing, Resources, Funding acquisition. ZM: Writing – review & editing, Investigation, Software. ML: Writing – review & editing, Software. RT: Visualization, Writing – review & editing. QZ: Visualization, Writing – review & editing. XL: Investigation, Writing – review & editing. LZ: Writing – review & editing, Investigation. SL: Software, Writing – review & editing.

Funding

The author(s) declare that financial support was received for the research and/or publication of this article. This research was funded by the Jiangsu Agricultural Science and Technology Innovation Fund (CX(22)2030), the central government guide local Science and Technology Development Fund Project Science and Technology Innovation Base Project (246Z7401G), North China Institute of Aerospace Engineering School-Level Innovation Funding Project (YKY-2024-92), and North China Institute of Aerospace Engineering School-Level Innovation Funding Project (KY202101). Science Research Project of Hebei Education Department (Grant No. QN2024113), North China Institute of Aerospace Engineering School-Level Innovation Funding Project (YKY-2024-86).

Conflict of interest

The authors declare that the research was conducted in the absence of any commercial or financial relationships that could be construed as a potential conflict of interest.

Generative AI statement

The author(s) declare that no Gen AI was used in the creation of this manuscript.

Publisher's note

All claims expressed in this article are solely those of the authors and do not necessarily represent those of their affiliated organizations, or those of the publisher, the editors and the reviewers. Any product that may be evaluated in this article, or claim that may be made by its manufacturer, is not guaranteed or endorsed by the publisher.

References

Alparslan, E., Coskun, H. G., and Alganci, U. (2009). Water quality determination of Küçükçekmece Lake, Turkey by using multispectral satellite data. *Sci. World J.* 9, 1215–1229. doi: 10.1100/tsw.2009.135

Bean, T. P., Greenwood, N., Beckett, R., Biermann, L., Bignell, J. P., Brant, J. L., et al. (2017). A review of the tools used for marine monitoring in the UK: combining historic and contemporary methods with modeling and socioeconomics to fulfill legislative needs and scientific ambitions. *Front. Mar. Sci.* 4:263. doi: 10.3389/fmars.2017.00263

Bi, R., Lu, Q., Yuan, T., Zhou, S., Yuan, Y., and Cai, Y. (2013). Electrochemical and spectroscopic characteristics of dissolved organic matter in a Forest soil profile. *J. Environ. Sci.* 25, 2093–2101. doi: 10.1016/S1001-0742(12)60283-6

Chen, Z. Y., and Li, S. Y. (2021). Seasonal variation of DOM spectral characteristics of Rivers with different urbanization levels in the three gorges reservoir area. *Huanjing Kexue* 42, 195–203. doi: 10.13227/j.hjkx.202004201

Chen, X., Sun, W., Jiang, T., and Ju, H. (2024). Enhanced prediction of river dissolved oxygen through feature- and model-based transfer learning. *J. Environ. Manag.* 372:123310. doi: 10.1016/j.jenvman.2024.123310

Chen, G., Wang, Y., Gu, X., Chen, T., Liu, X., Lv, W., et al. (2024). Estimating water quality parameters of freshwater aquaculture ponds using UAV-based multispectral images. *Agric. Water Manag.* 304:109088. doi: 10.1016/j.agwat.2024.109088

Cleophas, T. J., and Zwinderman, A. H. (Eds.) (2018). "Bayesian Pearson correlation analysis" in Modern Bayesian statistics in clinical research (Cham, Switzerland: Springer), 111–118. doi: 10.1007/978-3-319-92747-3_11

Duan, Y., Liu, L., Tang, R., Xie, S., Yang, M., Zhang, Z., et al. (2025). Assessing changes in China's pond water quality from 1989 to 2020: implications for green development in aquaculture. *Rev. Aquac.* 17:e12997. doi: 10.1111/raq.12997

Fu, B., Li, S., Lao, Z., Yuan, B., Liang, Y., He, W., et al. (2023). Multi-sensor and multi-platform retrieval of water chlorophyll a concentration in karst wetlands using transfer learning frameworks with ASD, UAV, and planet CubeSat reflectance data. *Sci. Total Environ.* 901:165963. doi: 10.1016/j.scitotenv.2023.165963

Galešić Divić, M., Kvesić Ivanković, M., Divić, V., Kišević, M., Panić, M., Lugonja, P., et al. (2026). Estimation of water quality parameters in oligotrophic coastal waters using Uncrewed-aerial-vehicle-obtained hyperspectral data. *J Mar Sci Eng* 11:11. doi: 10.3390/jmse11102026

Griffin, C. G., Frey, K. E., Rogan, J., and Holmes, R. M. (2011). Spatial and interannual variability of dissolved organic matter in the Kolyma River, East Siberia, observed using satellite imagery. *J. Geophys. Res. Biogeosci.* 116:G03018. doi: 10.1029/2010JG001634

Han, Y., Huang, J., Ling, F., Qiu, J., Liu, Z., Li, X., et al. (2023). Dynamic mapping of inland freshwater aquaculture areas in Jianghan plain, China. *IEEE J. Sel. Top. Appl. Earth Obs. Remote Sens.* 16, 4349–4361. doi: 10.1109/JSTARS.2023.3269430

He, J., Wu, X., Zhi, G., Yang, Y., Wu, L., Zhang, Y., et al. (2022). Fluorescence characteristics of DOM and its influence on water quality of rivers and lakes in the Dianchi Lake Basin. *Ecol. Indic.* 142:109088. doi: 10.1016/j.ecolind.2022.109088

Jeong, Y., Yu, J., Wang, L., Shin, H., Koh, S. M., and Park, G. (2018). Cost-effective reflectance calibration method for small UAV images. *Int. J. Remote Sens.* 39, 7225–7250. doi: 10.1080/01431161.2018.1516307

Kutser, T., Pierson, D. C., Tranvik, L., Reinart, A., Sobek, S., and Kõiv, T. (2005). Using satellite remote sensing to estimate the colored dissolved organic matter absorption coefficient in lakes. *Ecosystems* 8, 709–720. doi: 10.1007/s10021-003-0148-6

Li, C. Y., Huang, T. L., Wen, C. C., Liang, W. G., Lin, Z. S., Yang, S. Y., et al. (2021). Influence of storm runoff on the spectral characteristics of dissolved organic matter (DOM) in a drinking water reservoir during the flood season. *Huanjing Kexue* 42, 1391–1402. doi: 10.13227/j.hjkx.202007276

Liu, Y., Wang, Z., Yang, X., Wang, S., Liu, X., Liu, B., et al. (2023). Changes in Mariculture and offshore seawater quality in China during the past 20 years. *Ecol. Indic.* 157:111220. doi: 10.1016/j.ecolind.2023.111220

Liu, Y. J., Xia, K., Feng, H. L., and Fang, Y. M. (2019). Inversion of water quality elements in small and micro-size water region using multispectral image by UAV. *Acta Sci. Circumst.* 39, 1241–1249. doi: 10.13671/j.hjkxxb.2018.0362

Lumini, A., and Nanni, L. (2019). Deep learning and transfer learning features for plankton classification. *Ecol. Inform.* 51, 33–43. doi: 10.1016/j.ecoinf.2019.02.007

Luo, Y., Guo, N., Liu, D., Peng, S., Wang, X., and Wu, J. (2023). Inversion of water quality TN-TP values based on hyperspectral features and model validation. *Rev. Int. Géom.* 32, 39–52. doi: 10.32604/rig.2023.046014

Naylor, R. L., Hardy, R. W., Buschmann, A. H., Bush, S. R., Cao, L., Klinger, D. H., et al. (2021). A 20-year retrospective review of global aquaculture. *Nature* 591, 551–563. doi: 10.1038/s41586-021-03308-6

Ottinger, M., Bachofer, F., Huth, J., and Kuenzer, C. (2022). Mapping aquaculture ponds for the coastal zone of Asia with Sentinel-1 and Sentinel-2 time series. *Remote Sens* 14:153. doi: 10.3390/rs14010153

Peng, J., and Chen, B. (2024). Inversion of chlorophyll-a concentrations in Chaohu Lake based on GF-1 WFV images. *IEEE Access* 12, 24791–24802. doi: 10.1109/ACCESS.2024.3365288

Peng, Y., Sengupta, D., Duan, Y., Chen, C., and Tian, B. (2022). Accurate mapping of Chinese coastal aquaculture ponds using biophysical parameters based on Sentinel-2 time series images. *Mar. Pollut. Bull.* 181:113901. doi: 10.1016/j.marpolbul.2022.113901

Prasad, K. A., Ottinger, M., Wei, C., and Leinenkugel, P. (2019). Assessment of coastal aquaculture for India from Sentinel-1 SAR time series. *Remote Sens* 11:357. doi: 10.3390/rs11030357

Sagan, V., Peterson, K. T., Maimaitijiang, M., Sidike, P., Sloan, J., Greeling, B. A., et al. (2020). Monitoring inland water quality using remote sensing: potential and limitations of spectral indices, bio-optical simulations, machine learning, and cloud computing. *Earth-Sci. Rev.* 205:103187. doi: 10.1016/j.earscirev.2020.103187

Seidel, M., Hutengs, C., Oertel, F., Schwefel, D., Jung, A., and Vohland, M. (2020). Underwater use of a hyperspectral camera to estimate optically active substances in the water column of Freshwater Lakes. *Remote Sens* 12:1745. doi: 10.3390/rs12111745

Sibanda, M., Mutanga, O., Chimonyo, V. G. P., Clulow, A. D., Shoko, C., Mazvimavi, D., et al. (2021). Application of drone technologies in surface water resources monitoring and assessment: a systematic review of progress, challenges, and opportunities in the global south. *Drones* 5:84. doi: 10.3390/drones5030084

Singh, K. D., and Nansen, C. (2017). "Advanced calibration to improve robustness of drone-acquired hyperspectral remote sensing data" in Proceedings of the 2017 6th International Conference on Agro-Geoinformatics, Fairfax, VA, USA, 7–10 August 2017 (New York, NY, USA: IEEE), 1–6.

Wang, L., Yue, X., Wang, H., Ling, K., Liu, Y., Wang, J., et al. (2020). Dynamic inversion of inland aquaculture water quality based on UAVs-WSN spectral analysis. *Remote Sens* 12:402. doi: 10.3390/rs12030402

Weber, M., Auch, M., Doblander, C., Mandl, P., and Jacobsen, H.-A. (2021). Transfer learning with time series data: a systematic mapping study. *IEEE Access* 9, 165409–165432. doi: 10.1109/ACCESS.2021.3134628

Wu, H., Guo, Q., Zang, J., Qiao, Y., Zhu, L., and He, Y. (2021). Study on water quality parameter inversion based on Landsat 8 and measured data. *Remote Sens. Technol. Appl.* 36, 898–907. doi: 10.11873/j.issn.1004-0323.2021.4.0898

Xu, C., Su, G., Brosse, S., Zhao, K., Zhang, M., and Xu, J. (2024). Social benefits and environmental performance of aquaculture need to improve worldwide. *Commun. Earth Environ.* 5:698. doi: 10.1038/s43247-024-01790-0

Yao, K., Chen, Y., Li, Y., Zhang, X., Zhu, B., Gao, Z., et al. (2024). Water quality prediction of small-Micro water body based on the intelligent-algorithm-optimized support vector machine regression method and unmanned aerial vehicles multispectral data. *Sustain. For.* 16:559. doi: 10.3390/su16020559

Yao, Y., Wang, H., Yang, X., Gao, X., Yang, S., Zhao, Y., et al. (2025). Interpretable LAI fine inversion of maize by fusing satellite, UAV multispectral, and thermal infrared images. *Agriculture* 15:243. doi: 10.3390/agriculture15030243

Zhang, Y., Bleeker, A., and Liu, J. (2015). Nutrient discharge from China's aquaculture industry and associated environmental impacts. *Environ. Res. Lett.* 10:045002. doi: 10.1088/1748-9326/10/4/045002

Zhang, Y., Gao, G., Shi, K., Niu, C., Zhou, Y., Qin, B., et al. (2014). Absorption and fluorescence characteristics of rainwater CDOM and contribution to Lake Taihu, China. *Atmos. Environ.* 98, 483–491. doi: 10.1016/j.atmosenv.2014.09.038

Zhang, H., Ping, X., Wan, H., Luan, X., and Liu, F. (2024). Algae content prediction based on transfer learning and mean impact value. *Chemom. Intell. Lab. Syst.* 254:105244. doi: 10.1016/j.chemolab.2024.105244

Zhang, H., Yao, B., Wang, S., and Wang, G. (2021). Remote sensing estimation of the concentration and sources of Coloured dissolved organic matter based on MODIS: a case study of Erhai Lake. *Ecol. Indic.* 131:108180. doi: 10.1016/j.ecolind.2021.108180

Zheng, Z., Jiang, Y., Zhang, Q., Zhong, Y., and Wang, L. (2024). A feature selection method based on relief feature ranking with recursive feature elimination for the inversion of urban river water quality parameters using multispectral imagery from an unmanned aerial vehicle. *Water* 16:1029. doi: 10.3390/w16071029

Zhuang, F., Qi, Z., Duan, K., Xi, D., Zhu, Y., Zhu, H., et al. (2021). A comprehensive survey on transfer learning. *Proc. IEEE* 109, 43–76. doi: 10.1109/JPROC.2020.3004555